Inflation Experiments and Inverse Finite Element Modelling of Posterior Human Sclera

Brendan Geraghty[1*], Ahmed Abass[2], Ashkan Eliasy[2], Stephen W. Jones[2], Paolo Rama[3], Wael Kassem[4], Riaz Akhtar[2], Ahmed Elsheikh[2, 5, 6]

[1]Department of Musculoskeletal Biology, Institute of Ageing and Chronic Disease, University of Liverpool, L7 8TX, UK

[2]School of Engineering, University of Liverpool, Liverpool L69 3GH, UK

[3]Ophthalmology Department, San Raffaelle Scientific Institute, Milan, Italy

[4]Division of Construction Engineering, Umm Al-Qura University, College of Engineering at Al-Qunfudah, Al-Qunfudah 21912, Saudi Arabia

[5]National Institute for Health Research (NIHR) Biomedical Research Centre at Moorfields, Eye Hospital NHS Foundation Trust and UCL Institute of Ophthalmology, UK

[6]School of Biological Science and Biomedical Engineering, Beihang University, Beijing, China

***Author for correspondence:**

Brendan Geraghty, Department of Musculoskeletal Biology, Institute of Ageing and Chronic Disease, University of Liverpool, L7 8TX, UK

bren@liverpool.ac.uk

Keywords: human sclera, material properties, numerical simulation, finite element modelling, inverse analysis, ex-vivo experiments, stiffness, stress-strain behaviour

Financial Disclosure(s): None of the authors have financial disclosures.

Declaration of interest: None

Contributions:

A. Elsheikh designed and supervised the project. PR provided donor specimens. BG carried out the experiments, analysed the data, interpreted results and wrote the manuscript. WK analysed the results. AA analysed the results and edited the manuscript. RA, SJ and A. Eliasy interpreted the results and edited the manuscript. All authors have reviewed the manuscript, approved the final draft and provided a significant contribution to the study.

Number of words: 3,723 (excluding in-text citations)

Abstract

The complexity of inverse finite element modelling methods used in ocular biomechanics research has significantly increased in recent years in order to produce material parameters that capture microscale tissue behaviour. This study presents a more accessible method for researchers to optimise sclera material parameters for use in finite element studies where macroscale sclera displacements are required.

Five human donor sclerae aged between 36 and 72 years were subjected to cycles of internal pressure up to 61mmHg using a custom-built inflation rig. Displacements were measured using a laser beam and two cameras through a digital image correlation algorithm. Specimen-specific finite element models incorporating regional thickness variation and sclera surface topography were divided into six circumferential regions. An inverse finite element procedure was used to optimise Ogden material parameters for each region.

The maximum root mean squared (RMS) error between the numerical and experimental displacements within individual specimens was 17.5 μm. The optimised material parameters indicate a gradual reduction in material stiffness (as measured by the tangent modulus) from the equator to the posterior region at low-stress levels up to 0.005 MPa. The variation in stiffness between adjacent regions became gradually less apparent and statistically insignificant at higher stresses.

The study demonstrated how inflation testing combined with inverse modelling could be used to effectively characterise regional material properties capable of reproducing global sclera displacements. The material properties were found to vary between specimens, and it is expected that age could be a contributing factor behind this variation.

Introduction

Finite element (FE) modelling has long been recognised as a valuable tool for better understanding ocular response to mechanical actions. Many early studies focused on the cornea, where FE modelling was used to simulate the conditions caused by intraocular pressure (IOP) elevation or experienced in tonometry (Elsheikh and Wang, 2007), impact (Uchio et al., 1999), surgery (Alastrue et al., 2006, Fernandez et al., 2006) and disease (Gefen et al., 2009). Similarly, the behaviour of the sclera, the optic nerve head (ONH) and lamina cribrosa was the subject of several simulation studies due to their importance in the development and progression of glaucoma (Coudrillier et al., 2013, Downs et al., 2003, Eilaghi et al., 2010, Girard et al., 2009b, Girard et al., 2011, Grytz et al., 2014a, Sigal, 2009, Sigal et al., 2005).

In order to pursue the use of FE modelling as a tool in ophthalmology-related research, the ability to experimentally characterise the biomechanical behaviour of ocular tissues is of primary importance. Of the various test methods used, inflation is considered the most desirable owing to the similarity in loading mode experienced by the tissue when compared to in vivo intraocular pressure. Due to its anisotropic behaviour, complex geometry and variable wall thickness, inverse FE modelling has become an increasingly common method of determining sclera material properties. Since its first application in the field of ocular biomechanics by Woo et al. (1972), the complexity of inverse FE modelling methods have significantly increased. For instance, Girard et al. (2009c) developed an anisotropic hyperelastic constitutive model that predicted preferred collagen fibre orientation. Grytz and Meschke (2010) applied a method that also accounted for collagen crimp while Coudrillier et al. (2013) and Zhou et al. (2019) incorporated wide-angle x-ray scattering (WAXS) data of collagen fibril orientations. These intricate approaches allow for the characterisation of microscale behaviour of the sclera. However, implementation of the necessary processes can

be time consuming and the incorporation of collagen distribution data into an FE model requires technical user subroutines that are not always accessible to researchers.

This study aimed to produce a set of regional Ogden material parameters capable of predicting macroscale deformation behaviour of the sclera. Ex-vivo specimens were tested using a combination of experimental inflation, 2D digital image correlation (DIC) and inverse FE analysis. Specimen-specific FE meshes divided into six circumferential regions, each with an optimised pair of parameters capable of reproducing macroscale sclera displacements, were used in the inverse analysis. This approach accounts for the previously reported anterior to posterior variation in sclera material properties without the need to include detailed microstructure data thereby reducing the time required for data acquisition and post-test analysis. The presented methodology, and its results, can be used in FE studies where macroscale sclera displacements are apt.

Materials and Methods

Specimen Preparation

Five human donor sclerae were obtained fresh from the Fondazione Banca degli Occhi del Veneto, Italy. The average and standard deviation of the donors' age was 61.8±15.6 years (range 36 to 72 years). Routine screening was used to exclude donors with human immunodeficiency virus, hepatitis B and C, syphilis, central nervous system degenerative diseases, active infections, diabetes, eye tumours and glaucoma. The sclerae were not frozen at any stage. Ethical approval to use the specimens in research was obtained by the eye bank in accordance with the Declaration of Helsinki and its revisions up to 2013. The specimens were extracted approximately 6 hours after death, preserved in storage medium Eusol-C (Alchimia, Padova, Italy) and tested within 3 days post mortem. The limit of 3 days was based on the results of a previous experimental study confirming the maintenance of scleral tissue quality in the preservation medium Eusol-C for up to 5 days (Geraghty et al., 2012).

The sclerae were surgically detached from the cornea, extraocular muscles, retina and choroid. In order to assess if tissue swelling occurred during transit, nine thickness measurements were obtained between the anterior foramen and posterior pole post-enucleation by the eye bank using an UP-1000 ultrasound pachymeter (Nidek, Gamagori, Japan). The superior cardinal point on the anterior foramen edge and the measurement locations were marked using a gentian violet pen, as shown in Figure 1 (a) and (b). The measurements were repeated at the same locations before conducting the tests at the authors' laboratory using a Pachmate 55 (DGH Technologies, Exton, PA) with 5 μm accuracy. The average difference between the two sets of measurements was 4±25 μm, which is within the range previously reported for a comparison of conventional and handheld pachymeters (Queirós et al., 2007), thereby confirming that tissue swelling did not occur. The sclerae dimensions were measured using an electronic Vernier calliper (D00352, Duratool, Taiwan) with 10μm accuracy. The diameter of the anterior foramen after removal of the cornea was 17.75±0.64 mm, the specimen depth from the foramen edge to the posterior pole 19.54±0.45 mm and the equatorial diameter 24.26±0.38 mm, as shown in Figure 1 (b).

The superior, inferior, temporal and nasal (orthogonal) directions and the four 45° and 135° (diagonal) directions were marked on the anterior foramen edge of each specimen. The posterior pole was located by placing the specimens on their anterior foramen and marking the uppermost point on the posterior region. A flexible plastic strip marked with 2 mm increments was extended between the posterior pole and the anterior foramen to provide a guide for thickness measurements at 2 mm intervals along the eight meridians shown in Figure 1 (c) and (d). The pachymeter obtained 50 measurements per point and the average value was recorded. The regional thickness variation data obtained from this procedure was utilised in the generation of specimen-specific finite element meshes for the inverse analysis procedure.

Inflation testing

The sclerae were anatomically orientated and fixed along their anterior foramen using a specially designed clamping mechanism. The clamps provided a secure grip of the anterior sclera without the need for adhesives, as shown in Figure 2 (a). The clamped sclerae were filled with a saline solution before connection to an inflation test rig which was developed in an earlier study (Elsheikh et al., 2007). The specimens had a thin covering of the preservation medium Eusol-C upon removal from storage which prevented dehydration of the outer surface during testing.

Each specimen was subject to three cycles of internal pressure change from 1 mmHg up to 61 mmHg. Cyclic pressure changes were managed by means of a small reservoir whose vertical movement was computer-controlled and set to a pressure change rate of 37.5 mmHg/min. The pressure within the sclera was monitored using a differential pressure transducer (FDW, RDP Electronics, Wolverhampton, UK). Initial trials were carried out to assess the number of cycles required to produce repeatable pressure-displacement behaviour and the resulting tissue stiffness at maximum IOP. A significant difference was observed between the first and second cycle but little difference was observed thereafter. Consequently, the results of the third cycle were considered representative of stable material behaviour. Similar to previous studies on the mechanical properties of the sclera (Coudrillier et al., 2012, Fazio et al., 2012), all tests were carried out at room temperature (21°C).

Specimen Imaging

Displacement of the specimens was monitored along the orthogonal (superior-inferior and temporal-nasal) meridians of the sclera using two 14.7 MP digital cameras (Canon, Tokyo, Japan) with 4416 × 3312 pixels per image and orientated as shown in Figure 2 (b). Specimens were connected to the inflation rig ensuring alignment of the temporal-nasal and superior-inferior axes with the orthogonal planes. Prior to testing, a pulverised fuel ash powder was dispersed over the external surface of each sclera to enhance optical contrast. During the third

loading cycle, individual images with an accuracy of 12.6μm/pixel were taken at pressures of 1, 16, 31, 46 and 61mmHg using Remote Capture software (Canon, Tokyo, Japan).

2D digital image correlation (DIC) software (geoPIV8, Cambridge, UK) was used to analyse successive camera images and determine the movement of points on the sclera surface in the form of 2D displacement vectors measured in pixels. 1D posterior displacements along the ocular longitudinal axis were also continuously monitored using an LK-031 laser displacement sensor (Keyence, Milton Keynes, UK) with 1 μm accuracy. The laser displacement sensor measurements provided a means of calibrating the DIC software outputs to convert the displacements from pixels to millimetres. The resulting vectors obtained from the 2D DIC analysis were then used to produce pressure-displacement target curves for use in the inverse modelling procedure at the nine points located at 0°, 30° and 60° relative to the longitudinal axis on the superior-inferior and temporal-nasal meridians, as shown in Figure 2 (c) and (d).

Inverse Modelling Procedure

Sclera material behaviour parameters were derived from the experimental data using HEEDS Professional 5.2 (Red Cedar Technology, Michigan, USA), a design optimisation software, in conjunction with the nonlinear FE software Abaqus (Dassault Systèmes Simulia Corp., Rhode Island, USA). The SHERPA robust optimisation search algorithm, which is embedded in the optimisation software, was used. This algorithm spanned the parameter space while attempting to achieve convergence in targeted regions.

The FE mesh was generated using a custom written Visual Basic code (Microsoft, Redmond, WA) which utilised a diamatic dome configuration and consisted of one layer of 19661 fifteen-node C3D15H hybrid continuum elements. The FE meshes incorporated specimen-specific outer surface topography and sclera wall thickness variations. Due to the inability to measure the dimensions of the lamina cribrosa, this component was modelled as a group of six

elements occupying a circular area with 0.9 mm radius, 0.3 mm thickness, 0.3 MPa Young's modulus and centre located 2.7 mm away from the posterior pole (Saude, 1993, Sigal, 2009).

Movement of model nodes located on the anterior foramen was restrained in the three main directions, u, v and w, to simulate the conditions created by the mechanical clamps of the inflation rig. All other nodes possessed three degrees of freedom; displacement in u, v and w. Anterior to posterior variation of sclera material behaviour was enabled by dividing the model into 6 regions as illustrated in Figure 3, with region 1 being the most anterior and region 6 encompassing the posterior pole. Initial trials found 6 regions to be suitable for the current study as decreasing the number of regions reduced the accuracy of fit between the experimental and numerical results.

The SHERPA algorithm was used to determine a pair of first-order Ogden material parameters for each sclera region (see Appendix) by minimising the root mean square (RMS_{local}) error between the experimental and numerical posterior displacements at the nine targeted points on the sclera surface using the following objective function for each point where:

$$RMS_{local} = \sqrt{\frac{1}{P}.\sum_{p=1}^{P}(\delta_p^{exp} - \delta_p^{num})^2} \qquad \text{Equation 1}$$

where P is the total number of pressure levels at which the RMS is calculated (i.e. 16, 31, 46 and 61 mmHg), and δ_p^{exp} and δ_p^{num} represent the orthogonal components of the experimental and numerical displacements for a given point on the sclera surface at pressure level p. The optimisation algorithm also minimised RMS_{total}, the average of the local errors, where:

$$RMS_{total} = \frac{1}{N}\sum_{n=1}^{N} RMS_{local} \qquad \text{Equation 2}$$

where N is the total number of selected points on the scleral surface. Nodes in the FE mesh which corresponded to these locations were monitored and the optimisation software adjusted

the material parameters of each element group until the best possible fit was achieved between the experimental and numerical pressure-displacement results.

Statistical Analysis

The significance of associations between biomechanical properties (tangent modulus) and distance from posterior pole was assessed by Spearman rank correlation. The tests were performed in IBM SPSS Statistics 21 (IBM, Armonk, NY). $P<0.05$ was considered an indication of statistical significance.

Results

Experimental Results

All sclerae exhibited maximum thickness in the region of the posterior pole with values ranging between 1014 and 1108 μm (1076±23 μm). Thickness reduced progressively up to 6mm away from the posterior pole before reducing more rapidly down to a minimum of between 478 and 770 μm (630±76 μm) at 20 mm from the posterior pole. This was then followed by a rapid increase that continued to the edge of the anterior foramen (757±59 μm). Beyond 4-6 mm from the pole, measurements taken along the diagonal meridians exhibited greater thickness than the orthogonal meridians, however, all lines followed the same thickness variation pattern. These values were used to produce contour maps of the thickness variation over a developed scleral surface and the average of all specimens is shown in Figure 4. The maps were realised by creating a Delaunay triangulation between the thickness measurement locations and applying a cubic interpolation function within these regions.

Pressure-displacement behaviour for an example specimen is plotted in Figure 5 (a) and gives a direct comparison of the change in behaviour over three cycles. All specimens exhibited nonlinear pressure-displacement behaviour up to a pressure of between 20 and 30 mmHg. Beyond this level of internal pressure, the behaviour became almost linear. Progression from

the first to second loading cycle exhibited a notable stiffness increase in all specimens of 34±10% on average over the pressure range. A similar comparison between the second and third cycles showed that the stiffness increase reduced to 5±4%. Initial trials involving four loading cycles yielded only a further 3±4% stiffness increase between the third and fourth cycles, which justified the use of third cycle results as representative of the specimens' repeatable behaviour. Displacements at the posterior pole for all specimens during the third loading cycle ranged between 46 and 126 μm (90±26 μm) at 16 mmHg up to between 116 and 220 μm (191±54 μm) at 61 mmHg. Average behaviour observed during the third loading cycle for all specimens is shown in Figure 5 (b).

Analysis of specimen deformation using DIC demonstrated a gradual reduction in posterior displacement towards the equatorial region from a maximum at the posterior pole, Figure 6. At the maximum pressure applied, displacement of the transverse plane (temporal-nasal meridian) points positioned at 30° and 60° relative to the longitudinal axis were 155±15μm and 113±17μm, respectively. The corresponding points on the sagittal plane (superior-inferior) meridian experienced similar displacements of 160±15μm and 118±19μm.

Numerical Results

Following optimisation, the FE models demonstrated the same progressive increase in posterior displacement that was evident in the specimens during the experimental stage of the study, Figure 7. An example comparison of experimental displacements at the 9 points on Specimen 5 at which displacements were monitored, and those produced by the corresponding numerical model is shown in Figure 8. The comparison shows that model predictions closely matched the experimental results. The average errors for all specimens at the 9 points on the sclera when IOP was equal to 16, 31, 46 and 61mmHg were 8±7μm, 8±7μm, 10±8μm, and14±10μm, respectively.

The material parameters obtained for all specimens (see Table 1 in Appendix) were used to enable comparisons between the tangent modulus values, as calculated from circumferential stress-strain behaviour, in different regions relative to those around the posterior pole, Figure 9. The comparisons were held at four stress levels; 0.001, 0.005, 0.01 and 0.1 MPa, and it was clear that under low stresses (up to 0.005 MPa) there was a gradual reduction in tissue stiffness towards the posterior pole. For three of the five specimens, this reduction in stiffness was statistically significant at the 0.01 level. However, as the stress levels increased, the differences in stiffness between the six regions became gradually less apparent and statistically insignificant. The average circumferential stress-strain and tangent modulus-stress behaviour over the six regions for all specimens is presented in Figure 10.

Discussion

This study presents a novel method of optimising regional material properties capable of replicating global displacements, as measured at nine target points, from experimental inflation testing of human sclerae using 2D DIC and inverse FE modelling. Specimen-specific FE meshes incorporating regional thickness and topography variations were constructed using elements divided into six circumferential regions. Each region was assigned a first-order Ogden constitutive material model, the parameters of which were optimised in order to minimise RMS errors of pressure-displacement behaviour at locations in the FE models that corresponded to the nine target points on the sclera surface. The maximum RMS error between the experimental and numerical displacements within individual specimens was 17.5μm, demonstrating the ability of this method to obtain material behaviour parameters for ophthalmology-related FE research studies where macroscale sclera displacements are required.

The experimental protocol subjected human sclerae to cycles of internal pressure up to 61 mmHg to assess global displacements beyond the normal physiological and elevated pressure ranges typically seen in glaucoma. The pressure-displacement behaviour observed

during the inflation tests closely matched the nonlinear behaviour observed in similar testing scenarios for human (Fazio et al., 2012, Pyne et al., 2014, Tang et al., 2013, Woo et al., 1972), monkey (Girard et al., 2009a, Girard et al., 2009b) and porcine (Girard et al., 2008) sclera. Variations in pressure-displacement behaviour observed between different specimens could be partly attributed to the age variation between donor specimens used in this study (Coudrillier et al., 2015a).

All specimens demonstrated considerable thickness variation with maximum values in the vicinity of the posterior pole, reducing to a minimum close to the equator before increasing towards the anterior foramen. Similar to earlier studies (Elsheikh et al., 2010, Norman et al., 2010), measurements along the orthogonal meridians demonstrated reduced thickness compared to the diagonal meridians, however, all lines followed the same overall trend. The biomechanical behaviour results show a consistent trend of gradual stiffness reduction from the equator towards the posterior pole. While the trend was clear and statistically significant ($P=0.01$) for the majority of specimens at low stresses up to 0.005 MPa, it became less apparent and statistically insignificant under larger stresses for all specimens.

Various approaches have been used in inverse FE analyses of the posterior sclera. In a study carried out by Woo et al. (1972), the sclera was modelled as a single set of isotropic elements and their material behaviour was adjusted to fit a trilinear behaviour curve. In the work of Girard et al. (2009c), the posterior sclera was divided into nine sub-regions. Four sub-regions were orientated around the peripheral sclera, four around the parapapillary sclera and one around the optic disc and preferred fibre orientations were optimised for each region. In the work of Coudrillier et al. (2013), particular attention was given to the region spanning from the optic nerve to the mid-peripheral sclera where specimen-specific information on collagen orientations was obtained using WAXS. DIC-measured displacements were then applied as kinematic boundary conditions around this region in their models. A more recent study by Kollech et al. (2019) applied a different approach where sub-regions of the sclera were defined

based on first principal strains, as measured using sequential DIC. Inverse FE analysis was then used to optimise Holzapfel anisotropic material parameters within each sub-region.

The aforementioned advances in ophthalmology-related inverse FE modelling have provided valuable insights into the effects of scleral anisotropy (Coudrillier et al., 2013, Girard et al., 2009b, Grytz et al., 2014a), age-related stiffening (Coudrillier et al., 2015a, Coudrillier et al., 2012, Girard et al., 2009a), diabetes (Coudrillier et al., 2015b), race (Grytz et al., 2014b) and chronic IOP elevation (Coudrillier et al., 2015c, Girard et al., 2011). The inclusion anisotropic material properties are undoubtedly necessary for FE studies that aim to investigate the mechanical response of the optic nerve head. While variations in the mechanical properties of the lamina cribrosa have been shown to have little effect on the surrounding sclera (Girard et al., 2009b), the removal of anisotropy from the peripapillary region can significantly affect the behaviour of the sclera canal and lamina cribrosa (Coudrillier et al., 2013). However, in studies where microscale sclera displacements are not required such as design optimisation of ophthalmology-related medical devices or corneal studies where only global sclera displacement behaviour is important, our methodology can be applied to obtain suitable material parameters for use in FE models.

There are a number of limitations related to this study. Firstly, the same clamping mechanism was used in all inflation tests. In addition to the fixed boundary conditions created by the clamps, the use of a single clamp size coupled with the inter-specimen variation in sclera diameter (24.26±0.38 mm) would be expected to induce non-physiological stresses within the adjacent tissue. While this impacted the overall posterior displacement of the sclera, a trial carried out using FE analysis found the fixed boundary effects within the tissue to have diminished by the specimen equator.

Secondly, the FE model was based on a number of assumptions which could have affected the accuracy of its predictions. The division of the sclera into circumferential regions, although

361 justified by the approximately circumferential orientation of the displacement contour lines
362 (Figure 6), ignored possible variations in the scleral microstructure. A related limitation is the
363 assumption of isotropic sclera material behaviour in the FE models. This assumption, which
364 was necessary because of the same lack of information on scleral microstructure, was based
365 on a study in which the posterior sclera behaviour was found to be almost isotropic with the
366 average difference in stiffness between two orthogonal loading directions limited to 6%.
367
368 Thirdly, target curves used in the inverse modelling procedure were obtained from points along
369 the orthogonal meridians only. Consequently, and in contrast to studies that used fibre
370 reinforced models (Coudrillier et al., 2013, Coudrillier et al., 2012, Grytz et al., 2014a, Pyne et
371 al., 2014), the optimised material parameters presented in this study provide a means of
372 simulating whole hemisphere behaviour but may not represent more local behaviour at points
373 on the sclera shell between the meridians. Similarly, the finite element models were based on
374 the thickness measurements along the orthogonal and diagonal meridian lines, and
375 interpolation of thickness values was necessary for the areas between the meridian lines. It is
376 difficult to estimate the effect of this approximation on the model's predictions, but it is unlikely
377 to be significant. A further approximation was the simple and standard form assumed for the
378 lamina cribrosa, which was necessary due to our inability to distinguish between the nerve
379 fibres and scleral tissue and to measure the dimensions of the lamina cribrosa. While these
380 limitations, combined, are expected to have an effect on the FE predictions of the distribution
381 of stress, strain and deformation, they are unlikely to have a notable effect on overall
382 behaviour.
383
384 Finally, the loading regime adopted in this study was similar to those followed by other
385 researchers (Danielsen, 2004, Girard et al., 2009a, Schultz et al., 2008, Zeng et al., 2001)
386 where no recovery was included between the conditioning cycles and the specimens were not
387 allowed to creep before the final loading cycle. However, it is recognised that other studies
388 introduced different loading regimes incorporating recovery and creep and this could have an

effect on the obtained behaviour (Boyce et al., 2008). In particular, it has been argued that without recovery time the behaviour is likely to be affected by the strain history of preconditioning cycles (Carew et al., 2000). In appreciation of the potential importance of these effects, further tests will be conducted in which variations in the loading regime, including protocols to assess viscoelasticity, will be introduced to assess their effect on the obtained behaviour.

Conclusion

The study demonstrated how inflation testing combined with inverse modelling could be used to effectively characterise regional material properties of ocular tissue using circumferential regions of isotropic elements to replicate macroscale sclera displacements. The material properties were found to vary between specimens, and it is expected that age could be a contributing factor behind this variation. While this study laid out the experimental and inverse modelling procedures and presented overall behaviour patterns, follow up studies will attempt to characterise the variation in properties of scleral tissue with age and medical history.

References

ALASTRUE, V., CALVO, B., PENA, E. & DOBLARE, M. 2006. Biomechanical modeling of refractive corneal surgery. *J Biomech Eng,* 128**,** 150-60.

BATTAGLIOLI, J. L. & KAMM, R. D. 1984. Measurements of the compressive properties of scleral tissue. *Investigative Ophthalmology and Visual Science,* 25**,** 59-65.

BOYCE, B. L., GRAZIER, J. M., JONES, R. E. & NGUYEN, T. D. 2008. Full-field deformation of bovine cornea under constrained inflation conditions. *Biomaterials,* 29**,** 3896-3904.

CAREW, E. O., BARBER, J. E. & VESELY, I. 2000. Role of preconditioning and recovery time in repeated testing of aortic valve tissues: validation through quasilinear viscoelastic theory. *Ann Biomed Eng,* 28**,** 1093-100.

COUDRILLIER, B., BOOTE, C., QUIGLEY, H. A. & NGUYEN, T. D. 2013. Scleral anisotropy and its effects on the mechanical response of the optic nerve head. *Biomechanics and Modeling in Mechanobiology,* 12**,** 941-963.

COUDRILLIER, B., PIJANKA, J., JEFFERYS, J., SORENSEN, T., QUIGLEY, H. A., BOOTE, C. & NGUYEN, T. D. 2015a. Collagen Structure and Mechanical Properties of the Human Sclera: Analysis for the Effects of Age. *Journal of Biomechanical Engineering,* 137.

COUDRILLIER, B., PIJANKA, J., JEFFERYS, J., SORENSEN, T., QUIGLEY, H. A., BOOTE, C. & NGUYEN, T. D. 2015b. Effects of age and diabetes on scleral stiffness. *Journal of Biomechanical Engineering,* 137.

COUDRILLIER, B., PIJANKA, J. K., JEFFERYS, J. L., GOEL, A., QUIGLEY, H. A., BOOTE, C. & NGUYEN, T. D. 2015c. Glaucoma-related changes in the mechanical properties and collagen micro-architecture of the human sclera. *PLoS ONE,* 10.

COUDRILLIER, B., TIAN, J., ALEXANDER, S., MYERS, K. M., QUIGLEY, H. A. & NGUYEN, T. D. 2012. Biomechanics of the human posterior sclera: Age- and glaucoma-related changes measured using inflation testing. *Investigative Ophthalmology and Visual Science,* 53**,** 1714-1728.

DANIELSEN, C. C. 2004. Tensile mechanical and creep properties of Descemet's membrane and lens capsule. *Exp Eye Res,* 79**,** 343-50.

DOWNS, J. C., SUH, J. K., THOMAS, K. A., BELLEZZA, A. J., BURGOYNE, C. F. & HART, R. T. 2003. Viscoelastic characterization of peripapillary sclera: material properties by quadrant in rabbit and monkey eyes. *J Biomech Eng,* 125**,** 124-31.

EILAGHI, A., FLANAGAN, J. G., SIMMONS, C. A. & ETHIER, C. R. 2010. Effects of scleral stiffness properties on optic nerve head biomechanics. *Annals of biomedical engineering,* 38**,** 1586-1592.

ELSHEIKH, A., GERAGHTY, B., ALHASSO, D., KNAPPETT, J., CAMPANELLI, M. & RAMA, P. 2010. Regional variation in the biomechanical properties of the human sclera. *Experimental Eye Research,* 90**,** 624-633.

ELSHEIKH, A. & WANG, D. 2007. Numerical modelling of corneal biomechanical behaviour. *Comput Methods Biomech Biomed Engin,* 10**,** 85-95.

ELSHEIKH, A., WANG, D., BROWN, M., RAMA, P., CAMPANELLI, M. & PYE, D. 2007. Assessment of corneal biomechanical properties and their variation with age. *Current Eye Research,* 32**,** 11-19.

FAZIO, M. A., GRYTZ, R., BRUNO, L., GIRARD, M. J. A., GARDINER, S., GIRKIN, C. A. & DOWNS, J. C. 2012. Regional variations in mechanical strain in the posterior human sclera. *Investigative Ophthalmology and Visual Science,* 53**,** 5326-5333.

FERNANDEZ, D. C., NIAZY, A. M., KURTZ, R. M., DJOTYAN, G. P. & JUHASZ, T. 2006. A finite element model for ultrafast laser-lamellar keratoplasty. *Ann Biomed Eng,* 34**,** 169-83.

GEFEN, A., SHALOM, R., ELAD, D. & MANDEL, Y. 2009. Biomechanical analysis of the keratoconic cornea. *Journal of the Mechanical Behavior of Biomedical Materials,* 2**,** 224-236.

GERAGHTY, B., JONES, S. W., RAMA, P., AKHTAR, R. & ELSHEIKH, A. 2012. Age-related variations in the biomechanical properties of human sclera. *Journal of the Mechanical Behavior of Biomedical Materials,* 16**,** 181-191.

GIRARD, M. J., DOWNS, J. C., BURGOYNE, C. F. & SUH, J. K. 2008. Experimental surface strain mapping of porcine peripapillary sclera due to elevations of intraocular pressure. *J Biomech Eng,* 130**,** 041017.

GIRARD, M. J., SUH, J. K., BOTTLANG, M., BURGOYNE, C. F. & DOWNS, J. C. 2009a. Scleral Biomechanics in the Aging Monkey Eye. *Invest Ophthalmol Vis Sci*.

GIRARD, M. J. A., DOWNS, J. C., BOTTLANG, M., BURGOYNE, C. F. & SUH, J. K. F. 2009b. Peripapillary and posterior scleral mechanics - Part II: Experimental and inverse finite element characterization. *Journal of Biomechanical Engineering,* 131.

GIRARD, M. J. A., DOWNS, J. C., BURGOYNE, C. F. & SUH, J. K. F. 2009c. Peripapillary and posterior scleral mechanics - Part I: Development of an anisotropic hyperelastic constitutive model. *Journal of Biomechanical Engineering,* 131.

GIRARD, M. J. A., FRANCIS SUH, J. K., BOTTLANG, M., BURGOYNE, C. F. & CRAWFORD DOWNS, J. 2011. Biomechanical changes in the sclera of monkey eyes exposed to chronic IOP elevations. *Investigative Ophthalmology and Visual Science,* 52**,** 5656-5669.

GRYTZ, R., FAZIO, M. A., GIRARD, M. J. A., LIBERTIAUX, V., BRUNO, L., GARDINER, S., GIRKIN, C. A. & CRAWFORD DOWNS, J. 2014a. Material properties of the posterior human sclera. *Journal of the Mechanical Behavior of Biomedical Materials,* 29**,** 602-617.

GRYTZ, R., FAZIO, M. A., LIBERTIAUX, V., BRUNO, L., GARDINER, S., GIRKIN, C. A. & DOWNS, J. C. 2014b. Age-and race-related differences in human scleral material properties. *Investigative Ophthalmology and Visual Science,* 55**,** 8163-8172.

GRYTZ, R. & MESCHKE, G. 2010. A computational remodeling approach to predict the physiological architecture of the collagen fibril network in corneo-scleral shells. *Biomechanics and Modeling in Mechanobiology,* 9**,** 225-235.

KOLLECH, H. G., AYYALASOMAYAJULA, A., BEHKAM, R., TAMIMI, E., FURDELLA, K., DREWRY, M. & GEEST, J. P. V. 2019. A subdomain method for mapping the heterogeneous mechanical properties of the human posterior Sclera. *Frontiers in Bioengineering and Biotechnology,* 7.

NORMAN, R. E., FLANAGAN, J. G., RAUSCH, S. M. K., SIGAL, I. A., TERTINEGG, I., EILAGHI, A., PORTNOY, S., SLED, J. G. & ETHIER, C. R. 2010. Dimensions of the human sclera: Thickness measurement and regional changes with axial length. *Experimental Eye Research,* 90**,** 277-284.

PYNE, J. D., GENOVESE, K., CASALETTO, L. & GEEST, J. P. V. 2014. Sequential-digital image correlation for mapping human posterior sclera and optic nerve head deformation. *Journal of Biomechanical Engineering,* 136.

QUEIRÓS, A., GONZÁLEZ-MÉIJOME, J. M., FERNANDES, P., JORGE, J., ALMEIDA, J. B. & PARAFITA, M. A. 2007. Technical note: Accuracy and repeatability of a new portable ultrasound pachymeter. *Ophthalmic and Physiological Optics,* 27**,** 190-193.

SAUDE, T. 1993. *Ocular Anatomy and Physiology,* London, Wiley-Blackwell.

SCHULTZ, D. S., LOTZ, J. C., LEE, S. M., TRINIDAD, M. L. & STEWART, J. M. 2008. Structural factors that mediate scleral stiffness. *Invest Ophthalmol Vis Sci,* 49**,** 4232-6.

SIGAL, I. A. 2009. Interactions between geometry and mechanical properties on the optic nerve head. *Invest Ophthalmol Vis Sci,* 50**,** 2785-95.

SIGAL, I. A., FLANAGAN, J. G. & ETHIER, C. R. 2005. Factors influencing optic nerve head biomechanics. *Investigative Ophthalmology and Visual Science,* 46**,** 4189-4199.

TANG, J., HART, R., ROBERTS, C., WEBER, P., PAN, X. & LIU, J. 2013. Regional variation of scleral strains measured on human whole globes using ultrasound speckle tracking. *Invest. Ophthalmol. Vis. Sci.,* 54**,** 54-.

UCHIO, E., OHNO, S., KUDOH, J., AOKI, K. & KISIELEWICZ, L. T. 1999. Simulation model of an eyeball based on finite element analysis on a supercomputer. *Br J Ophthalmol,* 83**,** 1106-11.

WOO, S. L., KOBAYASHI, A. S., SCHLEGEL, W. A. & LAWRENCE, C. 1972. Nonlinear material properties of intact cornea and sclera. *Exp Eye Res,* 14**,** 29-39.
ZENG, Y., YANG, J., HUANG, K., LEE, Z. & LEE, X. 2001. A comparison of biomechanical properties between human and porcine cornea. *J Biomech,* 34**,** 533-7.
ZHOU, D., ABASS, A., ELIASY, A., STUDER, H. P., MOVCHAN, A., MOVCHAN, N. & ELSHEIKH, A. 2019. Microstructure-based numerical simulation of the mechanical behaviour of ocular tissue. *Journal of the Royal Society Interface,* 16.

Figure Captions

Figure 1 (a) and (b) Schematic elevations of a sclera including (a) a view of specimen orientation from the anterior side after cornea removal, and (b) a view of specimen dimensions from the temporal side. Circular points = approximate locations of eye bank thickness measurements. (c) and (d) Schematic elevations of sclera wall thickness measurement locations obtained along eight meridians lines between the anterior foramen and posterior pole, including (c) a view from the temporal side, and (d) a view from the posterior side. PP = Posterior Pole, ON = Optic Nerve.

Figure 2 (a) Temporal view of a schematic cross-section through a clamped sclera showing direction of the laser displacement sensor, and (b) posterior view of the sclera showing the camera positions whereby camera 1 monitors the temporal-nasal meridian and camera 2 monitors the superior-inferior meridian. (c) and (d) Schematic elevations of sclera illustrating the numbered points at which posterior displacements were monitored, including (c) a view from the temporal side, and (d) a view from the posterior side. PP = Posterior Pole. ON = Optic Nerve.

Figure 3 (a) Nasal and (b) posterior illustration of the finite element mesh showing the six element groups used during the inverse modelling procedure. ONH = Optic Nerve Head

Figure 4 Contour map of thickness variation at 25 μm intervals on a developed scleral surface for (a) average data obtained from all sclerae tested, and (b) represents the locations of thickness measurements. Colour bar values are presented in micrometres (μm). The map centre represents the posterior pole. Maps continue to the anterior foramen edge. S = superior direction, I = inferior direction, N = nasal direction, T = temporal direction, ONH = optic nerve head.

Figure 5 Example pressure-displacement behaviour measured at the posterior pole for (a) a 58 year old donor specimen over three cycles (plotted from a point of zero displacement to allow direct comparison between cycles) and (b) average pressure-displacement behaviour during the third loading for all specimens.

Figure 6 Contour maps of posterior displacements in millimetres observed experimentally from camera 1 (superior view) for a 58 year old donor specimen.

Figure 7 Example of FE model-predicted posterior displacements in millimetres over the sclera surface for a 58 year old donor specimen. Reduced thickness section on left side of model represents the location of the lamina cribrosa.

Figure 8 Example of fit between experimental and numerical posterior displacements for a 58 year old donor (Specimen 5), obtained at the monitored points shown in Figure 2 (c) and (d) on the sclera surface.

Figure 9 Ratios for tangent modulus within each region (R1 to R6) of the sclera models relative to tangent modulus at the posterior pole (R6) when stress is equal to (a) 0.001 MPa, (b) 0.005 MPa, (c) 0.01 MPa, and (d) 0.1 MPa.

Figure 10 Average behaviour in the circumferential direction for each sclera showing (a) stress-strain and (b) tangent modulus-stress trends for the six regions. Error bars represent standard deviation.

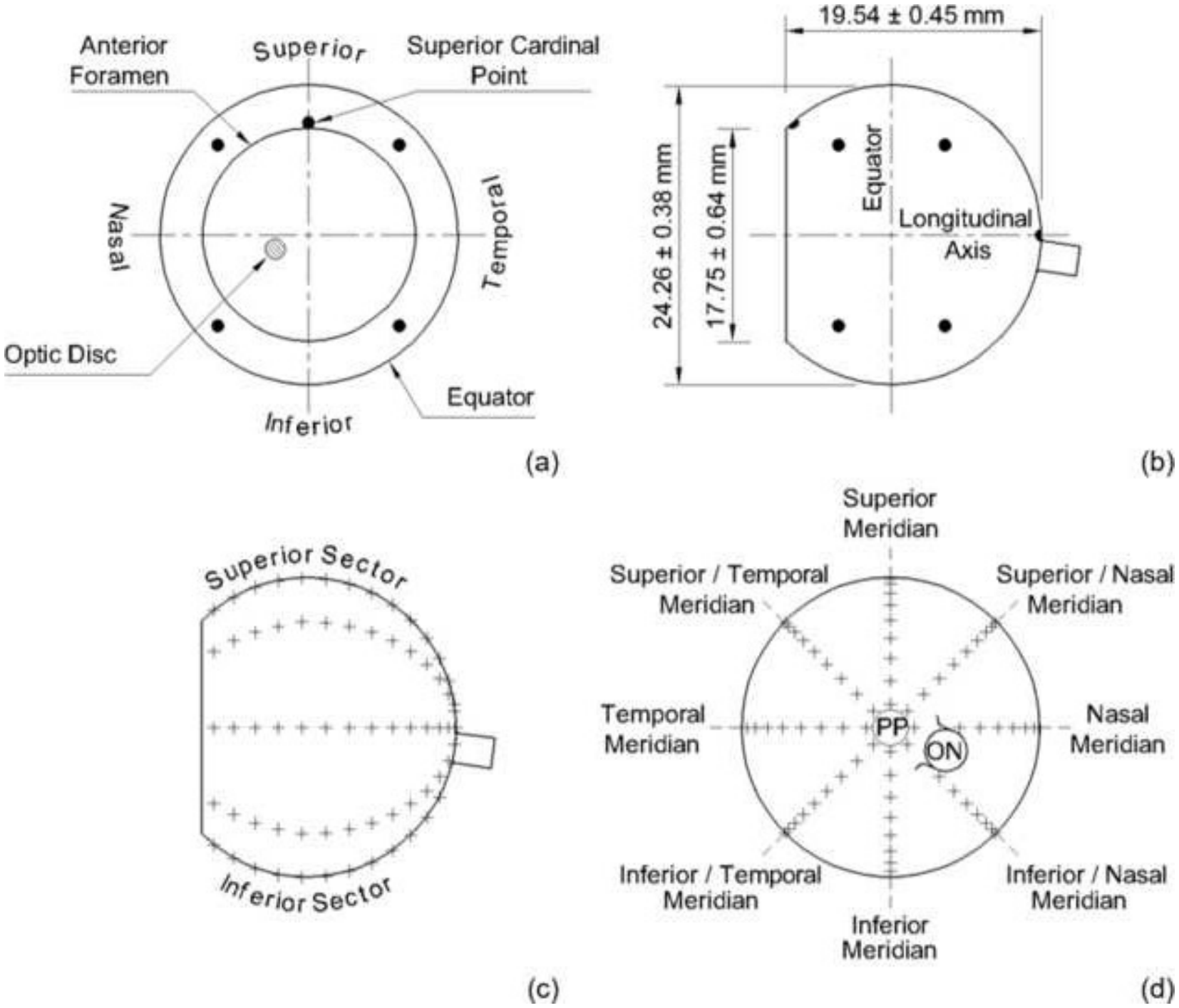

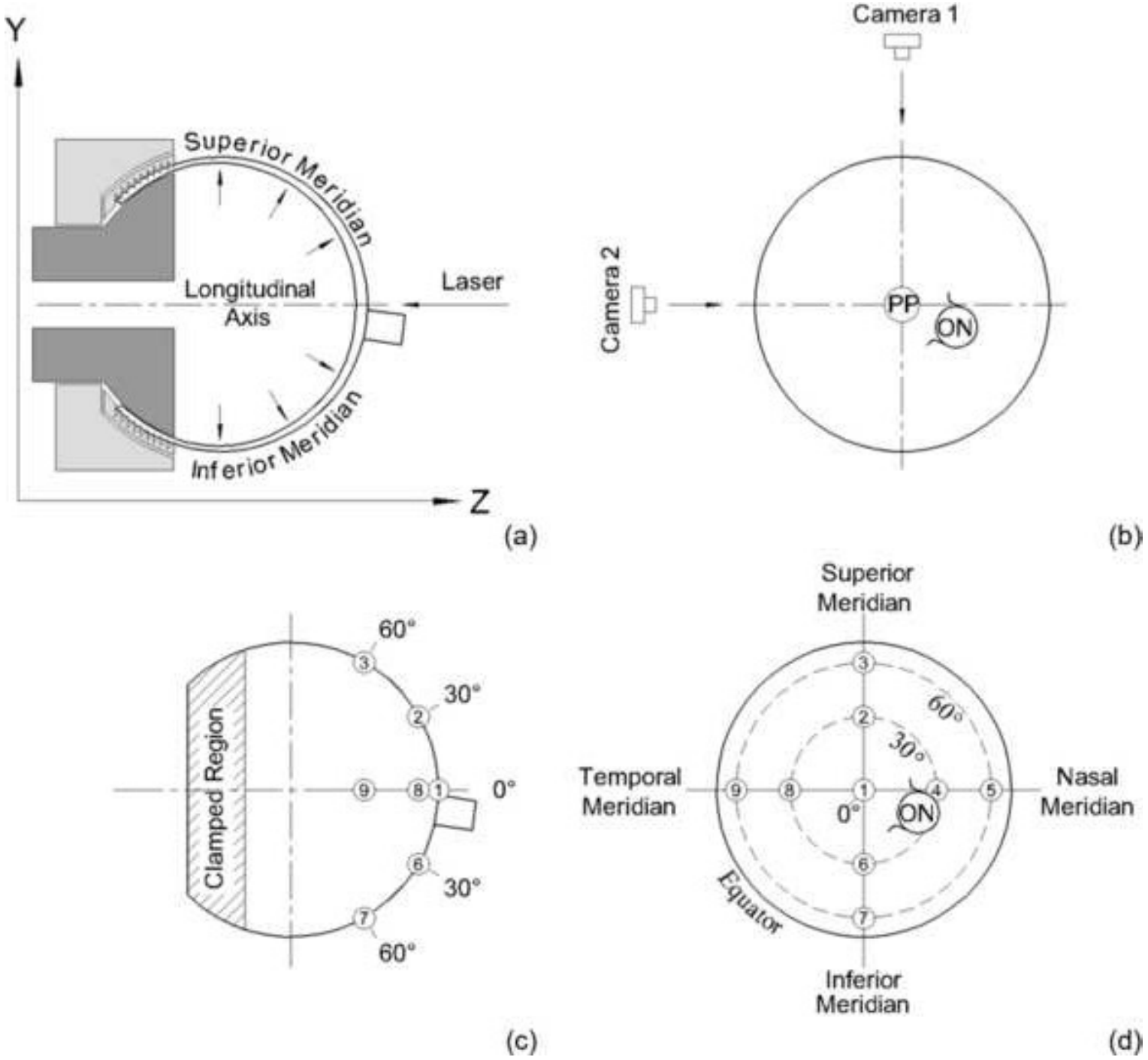

Figure_3

Click here to access/download;Figure;Fig_03.tif

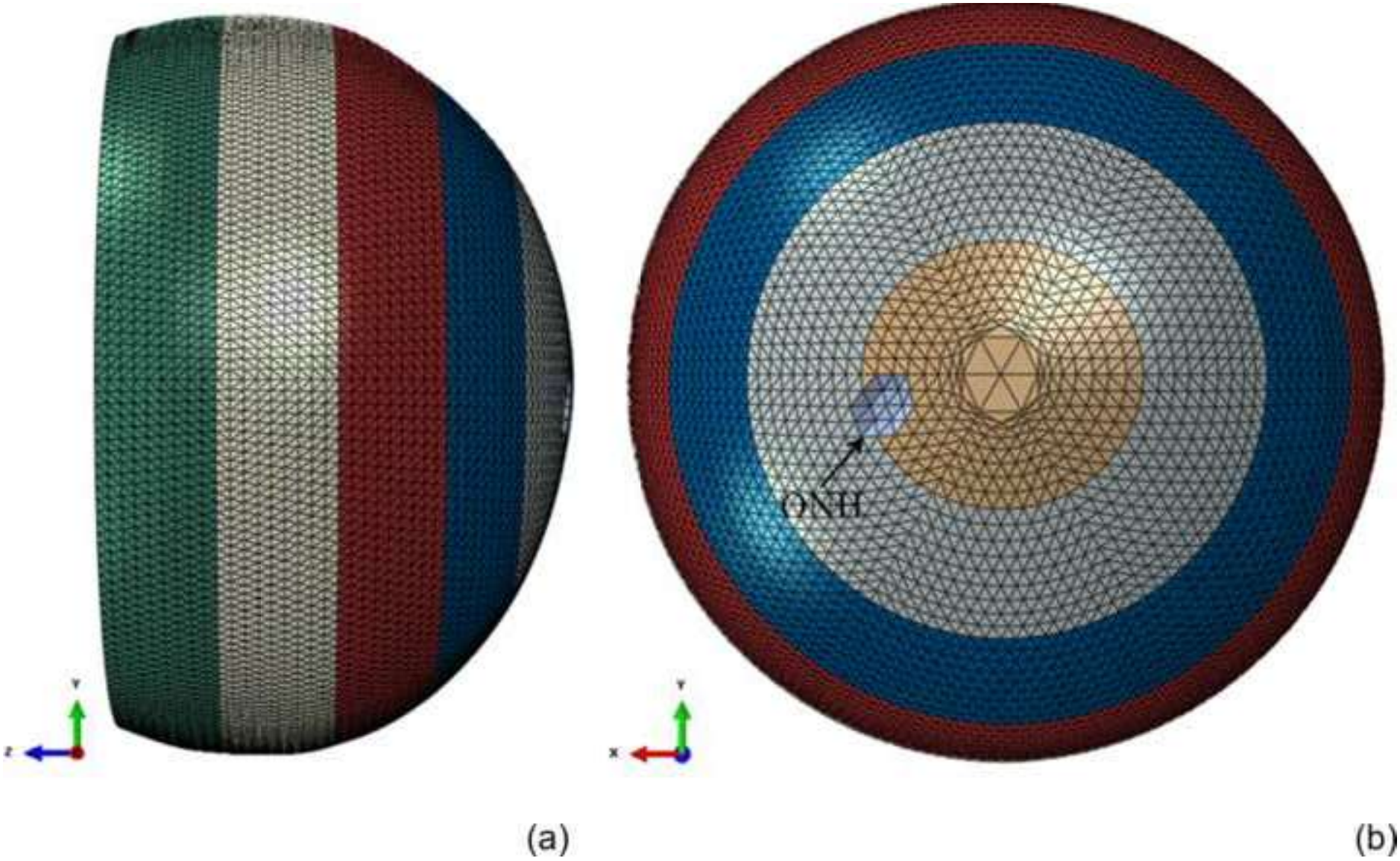

Figure_4

Click here to access/download;Figure;Fig_04.tif

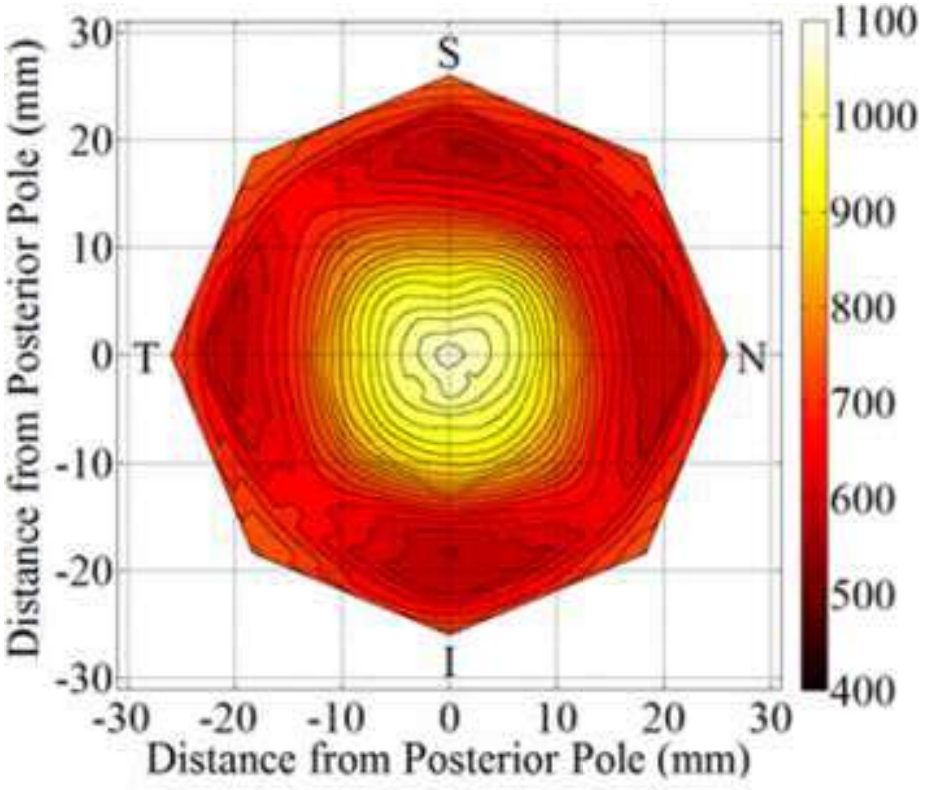

(a)

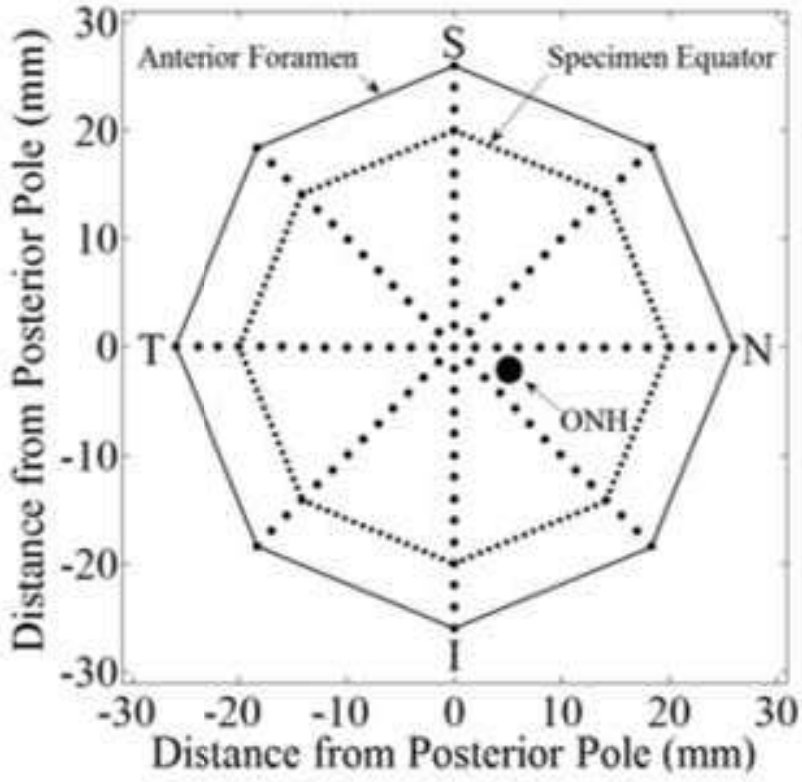

(b)

Figure_5

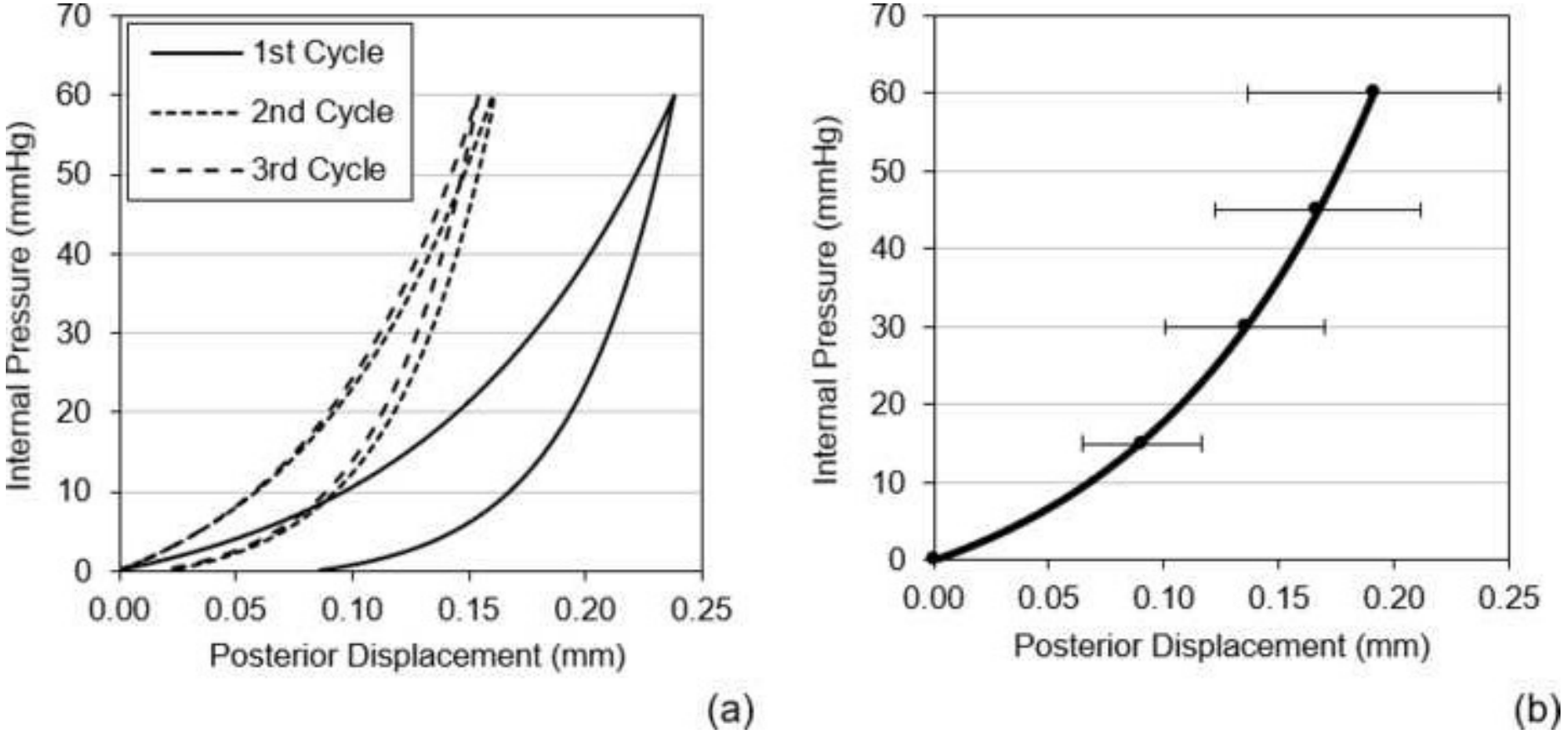

Figure_6

Click here to access/download;Figure;Fig_06.tif

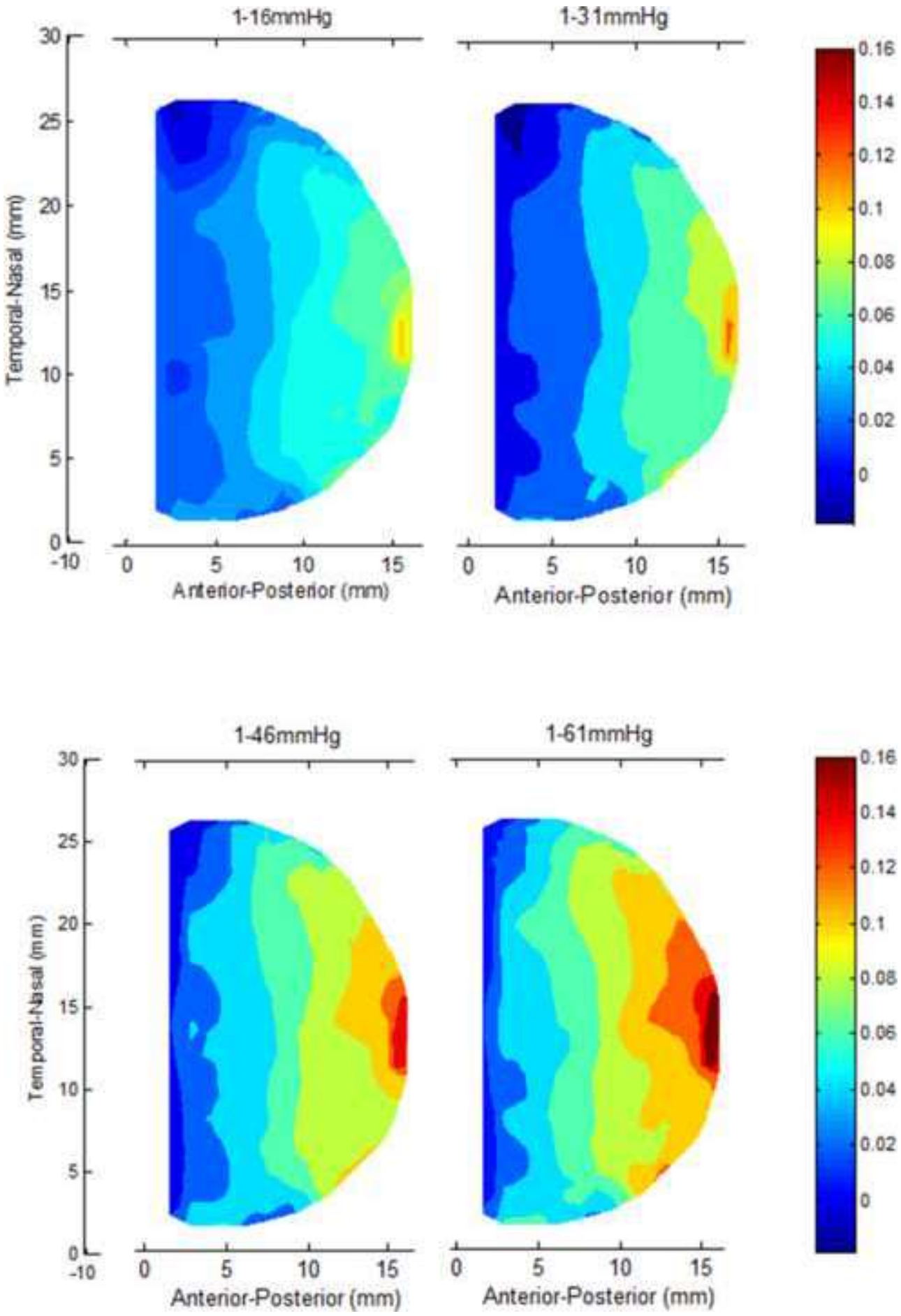

Figure_7

Click here to access/download;Figure;Fig_07.tif

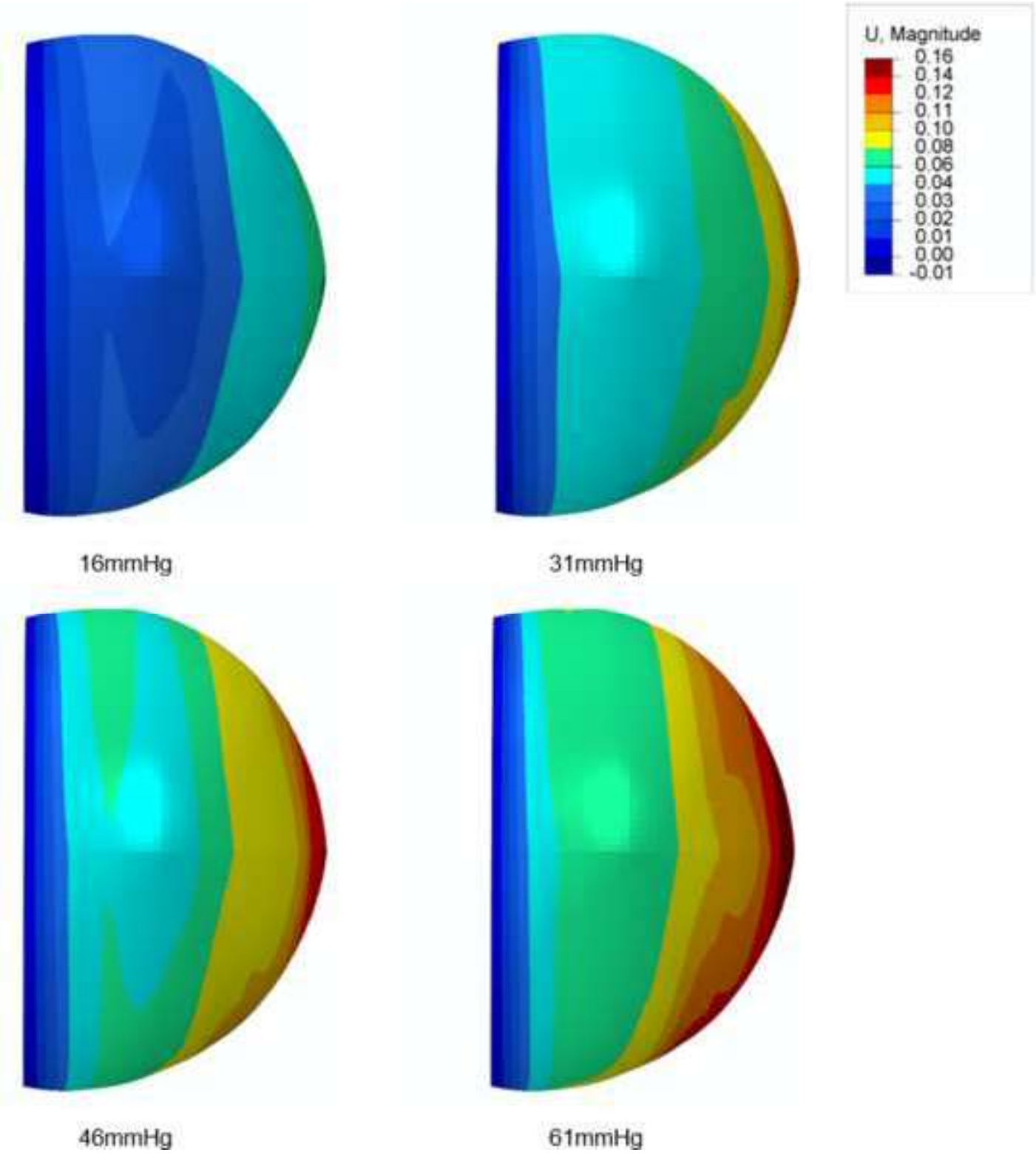

Figure_8

Click here to access/download;Figure;Fig_08.tif

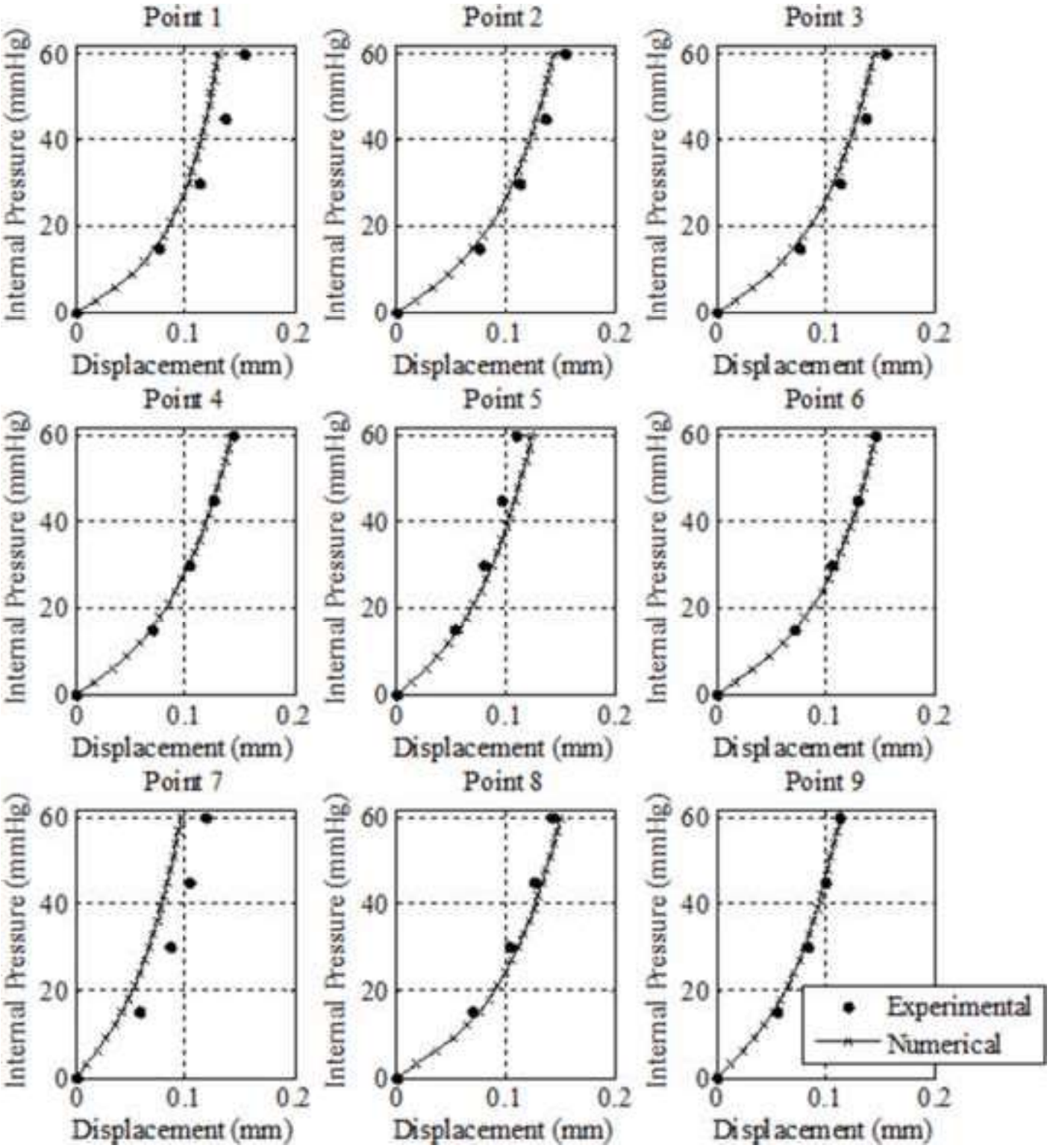

Figure_9

Click here to access/download;Figure;Fig_09.tif

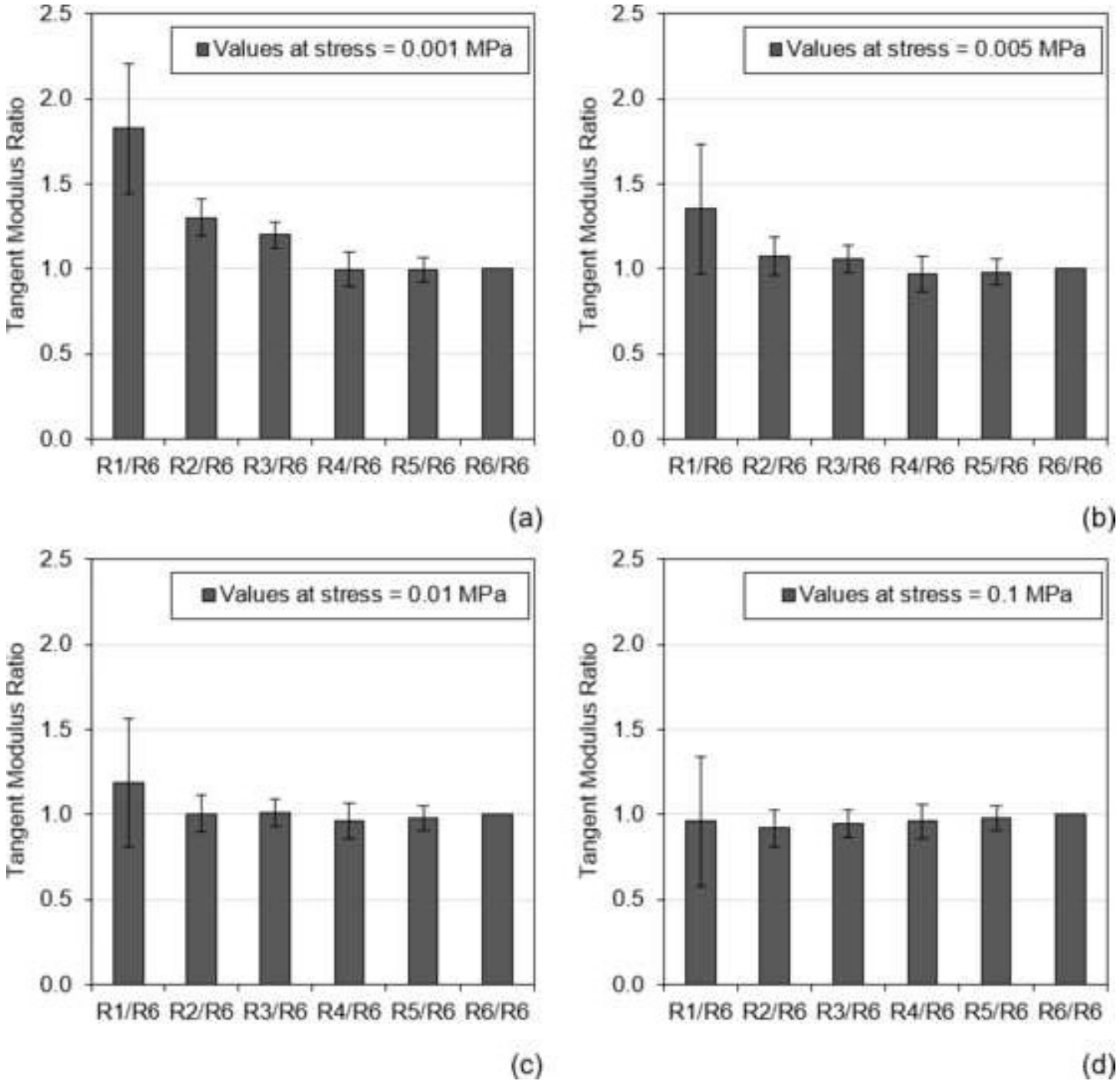

Figure_10

Click here to access/download;Figure;Fig_10.tif